J. Fluid Mech. (1971), *vol.* 45, *part* 2, *pp.* 395–415
Printed in Great Britain

Numerical simulation of developing and decaying two-dimensional turbulence

By D. K. LILLY

National Center for Atmospheric Research, Boulder, Colorado

(Received 21 November 1969 and in revised form 20 July 1970)

Two-dimensional isotropic turbulence is investigated in its development from an arbitrarily specified initial flow through its transformation into a statistically self-preserving decaying flow. Numerical simulation is the principal method of investigation. The early development is characterized by rapid growth of the mean squared vorticity gradient, and this growth is found to be predicted satisfactorily by the quasi-normal hypothesis. During the later states of decay the numerical results are found to be generally consistent with the predictions by Kraichnan, Leith and Batchelor of a k^{-3} inertial range spectrum. The dimensionless constant of the spectrum is found to be near 2, about half the value found earlier for turbulence maintained by a constant forcing amplitude. The results are also consistent with Batchelor's predictions of the time-dependent behaviour of certain quadratic moments: An inconsistency in those predictions is pointed out, however, which can be resolved by altering the inertial range spectrum by a logarithmic term, as suggested by Kraichnan. The most important two-point Eulerian correlation functions are exhibited. An investigation is made of the Gaussianity of the flow with results indicating a strong tendency toward intermittency in the enstrophy dissipation.

1. Introduction

The purpose of this paper is to describe the results of a series of numerical solutions of the Navier–Stokes equations which simulate the behaviour of developing and decaying two-dimensionally isotropic turbulence. The historical background of this work appears to be relatively short. Ogura (1952) studied the statistical properties of two-dimensional turbulence and (1958) applied some standard statistical methods to analysis of the large-scale atmosphere. He was evidently the first to notice the apparent k^{-3} spectrum of large-scale energy, but did not offer any explanation for it. Kraichnan (1967) pointed out the possibility of two inertial ranges in two-dimensional turbulence, a $k^{-\frac{5}{3}}$ spectrum range in which energy propagates to larger scales, and a k^{-3} range in which enstrophy (defined as half the mean-squared vorticity) propagates to smaller scales. He hypothesized that both ranges would exist simultaneously in continuously driven turbulence. Leith (1968), who had been working along somewhat similar lines, developed a closure hypothesis for two-dimensional turbulence which was consistent with both of the predicted inertial ranges. In a previous paper (Lilly 1969,

subsequently designated I), Kraichnan's hypothesis was shown to be consistent with the results of numerical simulation experiments designed to test it.

The present work was originally intended to test predictions of Batchelor (1969) and R. W. Bray (1966, unpublished thesis, Cambridge University) regarding the statistical behaviour of decaying two-dimensionally isotropic turbulent flow of large Reynolds number. After the major part of this work was completed it was noted that the early portions of the simulation solutions might be realistically interpreted in terms of earlier and simpler theories, and that agreement would constitute a partial check on the adequacy of the numerical methods employed. Some additional numerical experiments were then performed to clarify this point further.

2. The development of two-dimensional turbulence

For two-dimensional, incompressible, constant density and inviscid flow the Eulerian equations of motion and continuity can be replaced by an equation for ζ, the vertical component of vorticity, i.e.

$$\partial\zeta/\partial t + u_i\,\partial\zeta/\partial x_i = 0, \tag{1}$$

where u_i and ζ are related to a stream function ψ by

$$u_1 = -\partial\psi/\partial x_2, \quad u_2 = \partial\psi/\partial x_1, \quad \zeta = \partial^2\psi/\partial x_i^2. \tag{2}$$

It is well known that (1) and (2), together with closed or infinite boundary conditions, require the existence of two fundamental quadratic invariants, the spatial mean kinetic energy, $\bar{E}$, and the spatial mean enstrophy, $\bar{S}$, where these are defined as

$$\bar{E} = \tfrac{1}{2}\overline{u_i^2}, \quad \bar{S} = \tfrac{1}{2}\overline{\zeta^2}. \tag{3}$$

Of course all other functions of vorticity are similarly invariant. Orszag (private communication) has pointed out, however, that most of these functions are not invariant in a finite truncated Fourier mode representation of equations (1) and (2), nor are they so in any known finite difference scheme. Perhaps the simplest non-invariant quadratic form in two-dimensional flow is the mean-squared vorticity gradient, which in viscous flow is proportional to the rate of enstrophy dissipation. Batchelor (1969) noted that this quantity bears the same pivotal relationship to two-dimensional turbulence that vorticity itself does in three dimensions. We therefore base our analysis of the development of turbulence in two dimensions on the predicted rate of inviscid growth of $\overline{(\partial\zeta/\partial x_i)^2}$.

From (1) we can derive a relation for the generation of mean squared vorticity gradient in the form

$$\frac{1}{2}\frac{d}{dt}\overline{\left(\frac{\partial\zeta}{\partial x_i}\right)^2} = -\overline{\frac{\partial u_j}{\partial x_i}\frac{\partial\zeta}{\partial x_j}\frac{\partial\zeta}{\partial x_i}}. \tag{4}$$

The sign of the right-hand side cannot in general be predicted, and if the flow is initially Gaussian it must vanish. Upon differentiating (4) once more with respect to time and substituting the equations of motion and vorticity one obtains

$$\frac{d^2}{dt^2}\overline{\left(\frac{\partial\zeta}{\partial x_i}\right)^2} = \overline{\left(\frac{\partial u_j}{\partial x_i} + 2\frac{\partial u_i}{\partial x_j}\frac{\partial u_k}{\partial x_i} + \frac{\partial^2 p}{\partial x_j\partial x_k}\right)\frac{\partial\zeta}{\partial x_j}\frac{\partial\zeta}{\partial x_k}}. \tag{5}$$

The terms on the right side of (5) can in principle be evaluated in the case of the quasi-normal hypothesis, the assumption that fourth-order moments of velocity components or derivatives are related to second-order moments as if the components had Gaussian statistics. Thus if a, b, c and d are identified as velocity components or derivatives, the quasi-normality hypothesis predicts that

$$\overline{abcd} = \overline{ab}\,\overline{cd} + \overline{ac}\,\overline{bd} + \overline{ad}\,\overline{bc}. \tag{6}$$

Although Ogura (1962) and Kraichnan (1962) have shown that a consistent application of quasi-normality ultimately leads to unrealizable flow statistics, it is known that the hypothesis produces currect predictions for a short time interval after initiation from a Gaussian flow. Applying the above to (5) leads to vanishing of the second term on the right and evaluation of the first as

$$\overline{\frac{\partial u_j}{\partial x_i}\frac{\partial u_k}{\partial x_i}\frac{\partial \zeta}{\partial x_j}\frac{\partial \zeta}{\partial x_k}} = \overline{S}\overline{\left(\frac{\partial \zeta}{\partial x_i}\right)^2}. \tag{7}$$

By substitution of (7) into (5) we obtain therefore

$$\frac{d^2}{dt^2}\overline{\left(\frac{\partial \zeta}{\partial x_i}\right)^2} = 2\overline{S}\overline{\left(\frac{\partial \zeta}{\partial x_i}\right)^2} + 2\overline{\frac{\partial^2 p}{\partial x_j \partial x_k}\frac{\partial \zeta}{\partial x_j}\frac{\partial \zeta}{\partial x_k}}. \tag{8}$$

A similar expression was derived by Reid (1955) for the generation of mean-squared gradient (in three dimensions) of a scalar uncorrelated with the velocity field. In that case the term corresponding to the last of (8) was found to vanish. When the scalar is a vorticity component, however, the term does not vanish. It can be formally evaluated as a double integral of a product of velocity correlation functions. An equivalent and somewhat more useful expression for our purposes can be obtained by use of an integral involving the energy spectrum. The following derivation of this integral is due to Orszag (private communication).

Ogura (1962) and Kraichnan (1967) exhibited expressions for the rate of acceleration of the scalar energy spectrum for two-dimensional flow if the quasi-normal approximation and isotropy are assumed. Kraichnan (1970) has noted that his expression is too large by a factor of π. A correct and convenient expression can be derived from Ogura's equation (14) by symmetrizing it with respect to the dummy variables of integration to obtain

$$\frac{\partial^2 E(k)}{\partial t^2} = \frac{1}{\pi}\int_0^\infty \int_{|k-p|}^{k+p} \frac{Q}{kpq}(p^2-q^2)\left[\frac{(p^2-q^2)\,E(p)\,E(q)}{pq} + \frac{(k^2-p^2)\,E(k)\,E(p)}{kp} + \frac{(q^2-k^2)\,E(q)\,E(k)}{qk}\right] dq\,dp, \tag{9}$$

where

$$Q^2 = 2k^2p^2 + 2p^2q^2 + 2q^2k^2 - p^4 - q^4 - k^4. \tag{10}$$

The variables p, q and k are the magnitudes of a wave vector triad such that $\mathbf{p}+\mathbf{q}+\mathbf{k} = 0$. $E(k)$ is the scalar energy spectrum for two-dimensional flow.

The rate of acceleration of mean-squared vorticity gradient is

$$\frac{d^2}{dt^2}\overline{\left(\frac{\partial \zeta}{\partial x_i}\right)^2} = 2\int_0^\infty k^4 \frac{\partial^2 E(k)}{\partial t^2}\,dk. \tag{11}$$

Substitution of (9) into (11) leads to an integral expression which must be symmetric with respect to the wave vector amplitudes p, q and k. By interchanging the labels and re-arranging terms we make use of this symmetry to express the integral in a more convenient form, i.e.

$$\frac{d^2}{dt^2}\overline{\left(\frac{\partial\zeta}{\partial x_i}\right)^2} = \int_0^\infty \int_0^\infty \frac{(p^2-q^2)^2}{p^2q^2} E(p)\,E(q)\,I(p,q)\,dp\,dq, \tag{12}$$

where

$$I(p,q) = \frac{2}{\pi}\int_{|p-q|}^{p+q} \frac{Q}{k}\,[k^4-(p^2+q^2)\,k^2+p^2q^2]\,dk. \tag{13}$$

We now proceed to evaluate the inner integral, $I(p,q)$. If x is defined as the cosine of the angle opposite k in the k, p, q triangle, the law of cosines specifies that

$$k^2 = p^2+q^2-2pqx. \tag{14}$$

By differentiation of (14), holding p and q constant, we also obtain

$$dk = -(pq/k)\,dx. \tag{15}$$

By substitution of the above two expressions into (13) we replace the k integration by one over x and obtain

$$I(p,q) = \frac{4}{\pi}p^3q^3\int_{-1}^{1}\left[\frac{pq}{p^2+q^2-2pqx}-2x\right](1-x^2)^{\frac{1}{2}}\,dx, \tag{16}$$

where the limits on x correspond to the possible range of the angle opposite k, from 0 to π. The integral is now evaluated by elementary methods, with the part corresponding to the second term in brackets vanishing identically, and the result written

$$I(p,q) = p^2q^2[p^2+q^2-|p^2-q^2|]. \tag{17}$$

We now substitute (17) into (12), once again using the symmetry between p and q to eliminate the absolute value expression, with the result that

$$\frac{d^2}{dt^2}\overline{\left(\frac{\partial\zeta}{\partial x_i}\right)^2} = 4\int_0^\infty \int_0^p (p^2-q^2)^2 q^2 E(p)\,E(q)\,dq\,dp. \tag{18}$$

We have tested the above prediction for one specific case by means of a special numerical simulation experiment in which the inviscid vorticity equation is integrated for 100 time steps from an initial condition chosen to have a flat truncated scalar energy spectrum, i.e.

$$E(k) = E_1 = \text{constant for } k_0 \leqslant k \leqslant k_1 \text{ at time} = 0. \tag{19}$$

The initial stream field is composed of an ensemble of Fourier modes, whose amplitudes are randomly chosen from a Gaussian population with zero average and variance corresponding to (19). The wave-number limits k_0 and k_1 are taken to be 1 and 4 respectively. The outer limit is chosen as the closest possible approach to a circle in finite wave vector space. Five independent realizations are developed, in order to allow formation of an ensemble average.

The numerical methods utilized in obtaining the solutions are more fully described in I. Briefly, a cyclically symmetric square area is divided into 64×64

mesh boxes and the equation of vorticity, discretized at the centre of each mesh box, is solved by finite difference methods. The energy- and enstrophy-conserving difference scheme introduced by Arakawa (1966) is used for the non-linear terms. Time integration is performed by use of the second-order Adams–Bashforth method. The solution of the Poisson equation necessary to obtain stream function and velocity components from the vorticity is accomplished by a non-iterative method utilizing fast Fourier transforms.

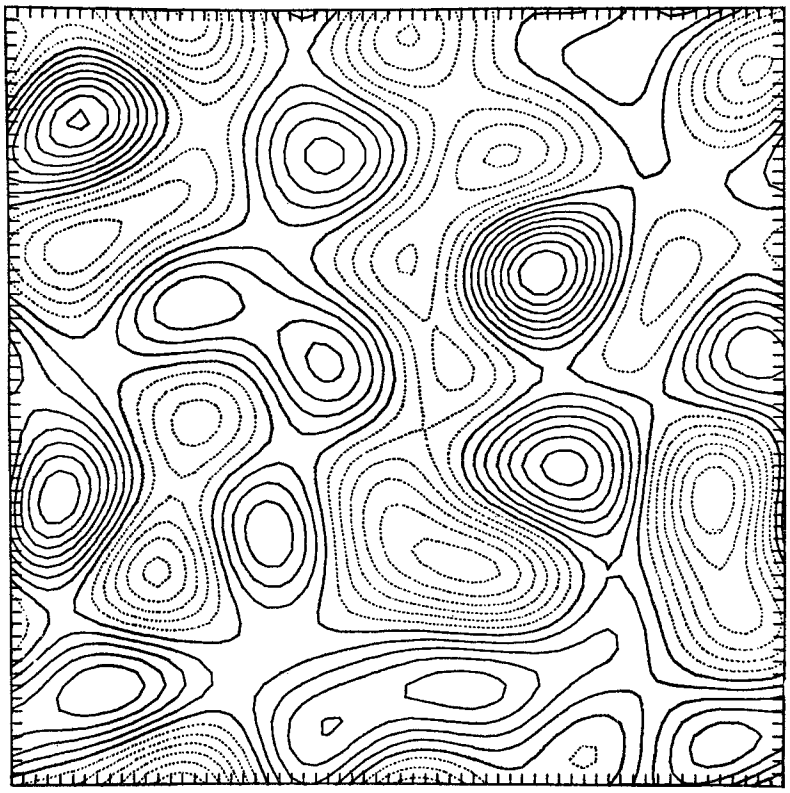

FIGURE 1. Map of the vorticity field at the initial time for one realization of the development experiment. The analysis is done by machine-coded linear interpolation from a mesh of 64 × 64 data points. The mesh interval is shown by hatch marks along the boundaries. The contours are drawn at uniform but arbitrarily selected intervals. Solid contours enclose areas of positive vorticity, dotted contours negative. The zero line is the first solid contour. The field is cyclically symmetric across all boundaries.

Figures 1 and 2 are maps of the vorticity field at the initial time and after 100 time steps, respectively, for one of the five realizations. They show clearly the self-distorting nature of the flow which leads to a general increase in the vorticity gradient amplitude. Figure 3 shows the growth of $\overline{(\partial\zeta/\partial x_i)^2}$ during the 100 time steps of each of the five realizations. The ordinate and abscissa have been made dimensionless by scaling by k_1 and the enstrophy, which remains constant during each realization. The time step is chosen for convenience to be constant and uniform in all realizations. In all cases it lies within the minimum

requirements for computational stability. The curves are each labelled according to the value of enstrophy which characterizes the corresponding realization.

The prediction of the quasi-normal theory at initial time is obtained by substituting (19) into (18) and integrating the latter to obtain

$$\frac{d^2}{dt^2}\overline{\left(\frac{\partial\zeta}{\partial x_i}\right)^2} = \tfrac{4}{105}E_1 k_1^8\left(1-\frac{3}{32}\frac{k_0^3}{k_1^3}+\ldots\right). \tag{20}$$

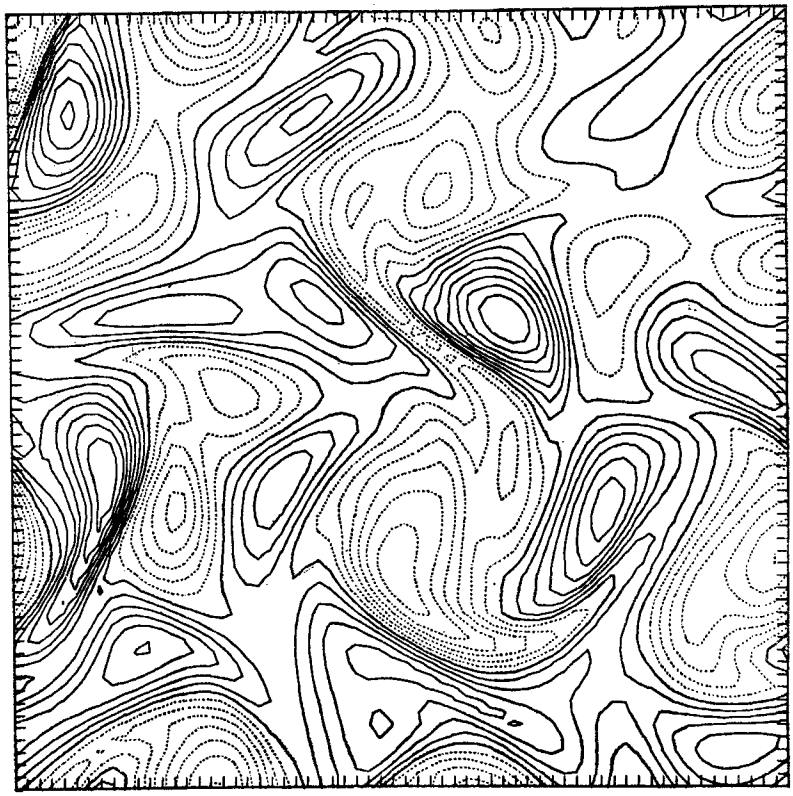

FIGURE 2. The vorticity field for the same realization after 100 time steps of integration of the inviscid vorticity equation. The vorticity maxima and minima remain essentially unchanged but the mean squared vorticity gradient has obviously increased.

Since enstrophy is a conservative quantity in this experiment it is useful to express the above result as a product of enstrophy and mean squared vorticity gradient, i.e. in the form of the first term in (8). After evaluating the appropriate integrals we obtain, in place of (20),

$$\frac{1}{2}\frac{d^2}{dt^2}\overline{\left(\frac{\partial\zeta}{\partial x_i}\right)^2} \approx 0{\cdot}131\bar{S}\overline{\left(\frac{\partial\zeta}{\partial x_i}\right)^2}. \tag{21}$$

If the initial trend of $\overline{(\partial\zeta/\partial x_i)^2}$ is nearly zero, as is expected with a sufficiently random initial flow field, (21) predicts that that quantity will start to grow like the hyperbolic cosine. From inspection of figure 3 it is apparent that the prediction of (21) is at least qualitatively fulfilled, although a rather large spread of

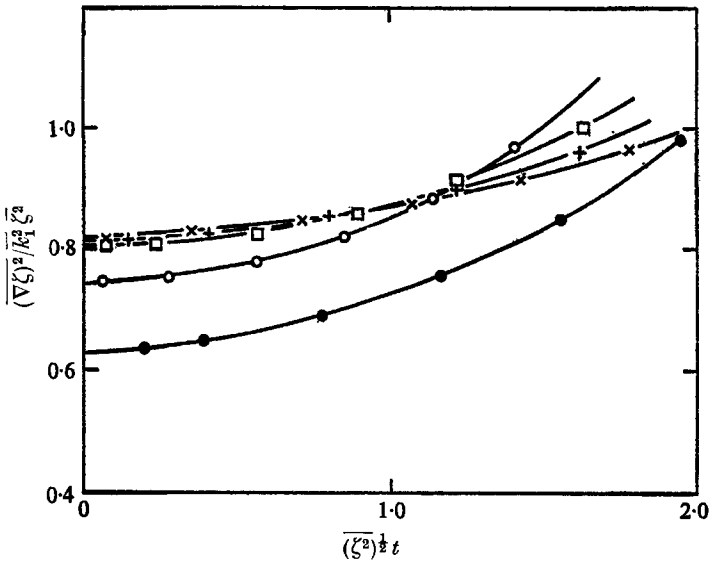

FIGURE 3. Mean-squared vorticity gradient plotted against time for 5 realizations of the development experiment. The ordinate and abscissa have been scaled by k_1, the maximum scalar wave-number of the Fourier modes contained in the initial flow field, and the mean-squared vorticity, which remains constant during each realization. Values of $\overline{\zeta^2}$: ●, 0·1568; ×, 0·1284; +, 0·1064; ○, 0·0813; □, 0·1070.

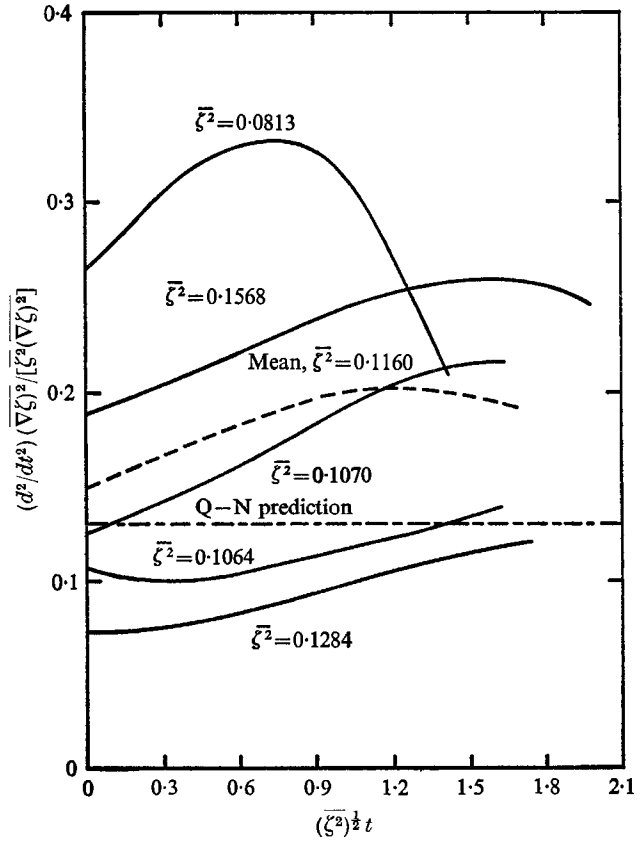

FIGURE 4. The squared exponential growth rate for growth of squared vorticity gradient plotted against time for the 5 realizations shown on figure 3. The mean of the 5 and the quasi-normal prediction at the initial time instant are also shown.

amplitudes of $\bar{S}$, $\overline{(\partial\zeta/\partial x_i)^2}$, and their growth rates exists between the different realizations.

To test the prediction more exactly the ratio $(d^2/dt^2)\,\overline{(\partial\zeta/\partial x_i)^2}/\bar{S}\,\overline{(\partial\zeta/\partial x_i)^2}$ is computed and plotted as a function of time for the five realizations on figure 4. The mean of the five realizations is shown as the dashed line and the quasi-normal prediction from (21), 0·131, is shown as the dash-dotted line. The mean and the predicted values differ at the initial time by not much more than the standard deviation of the mean, so that the prediction is reasonably well confirmed at the time when it should have its greatest validity. As time progresses, the result diverges from the prediction of quasi-normality, with an early tendency for faster growth rates. Toward the end of the experiment most of the realizations show a tendency for levelling off or decrease of the exponential growth rates. If the experiment were continued indefinitely with the disturbing effects of truncation and aliasing errors removed (they are negligible in the 100 step experiment), the ultimate result should be a two-dimensional equipartition spectrum, as described by Kraichnan (1967). At this point the mean-squared vorticity gradient would become constant but much larger than its value during the 100 step experiment.

3. The decay experiments

The initial stretching of the vorticity contours which leads to turbulent flow can be adequately described by inviscid dynamics. The later development of a complete statistical structure and its ultimate decay requires the introduction of viscous forces. The vorticity equation derived from the complete Navier–Stokes equations in two dimensions is

$$\frac{\partial\zeta}{\partial t}+u_i\frac{\partial\zeta}{\partial x_i}=\nu\frac{\partial^2\zeta}{\partial x_i^2}, \tag{22}$$

where ν is the coefficient of viscosity. For the decay experiments the initial flow field is produced by adding a forcing function to the right side of (22) for a limited number (less than 50) time steps, then turning it off and continuing the integration as if from an initially specified flow. The forcing function and the initial flow field resulting from it differ slightly from the initial flow described in the development experiments. The forcing function is constructed from a set of Fourier modes randomly chosen from a Gaussian population of amplitudes associated with wave vectors lying on the perimeter of a square in wave vector space. The half-width of the square is 8, so that the wave-number amplitudes of the modes comprising the initial flow condition lie between 8 and $8(2)^{\frac{1}{2}}$. Figure 5 is a map of the stream function at the end of the forcing period for the realization later designated by $R = 537$. A map of the vorticity looks very similar to that of the stream function with the signs reversed, since the fields are nearly monochromatic.

The upper curve in figure 6, labelled 'initial' shows the corresponding scalar energy spectrum. This spectrum, as with all others exhibited, is obtained by summing the squared amplitudes of the Fourier modes around boxes in wave vector space, rather than the circle integrals usually assumed in analytic theory. The motive for this procedure is mainly that of convenience, but there should be

no significant qualitative difference between the behaviour of the box-summed and circle-summed spectra. In particular, a power-law distribution in one case translates to the same power law in the other.

Initial conditions for the two other realizations to be described differ from the above in both the flow details, because of a different random choice of Fourier mode amplitudes in the forcing function, and in the total energy content, because of variation in the length of time the forcing function is allowed to operate. The

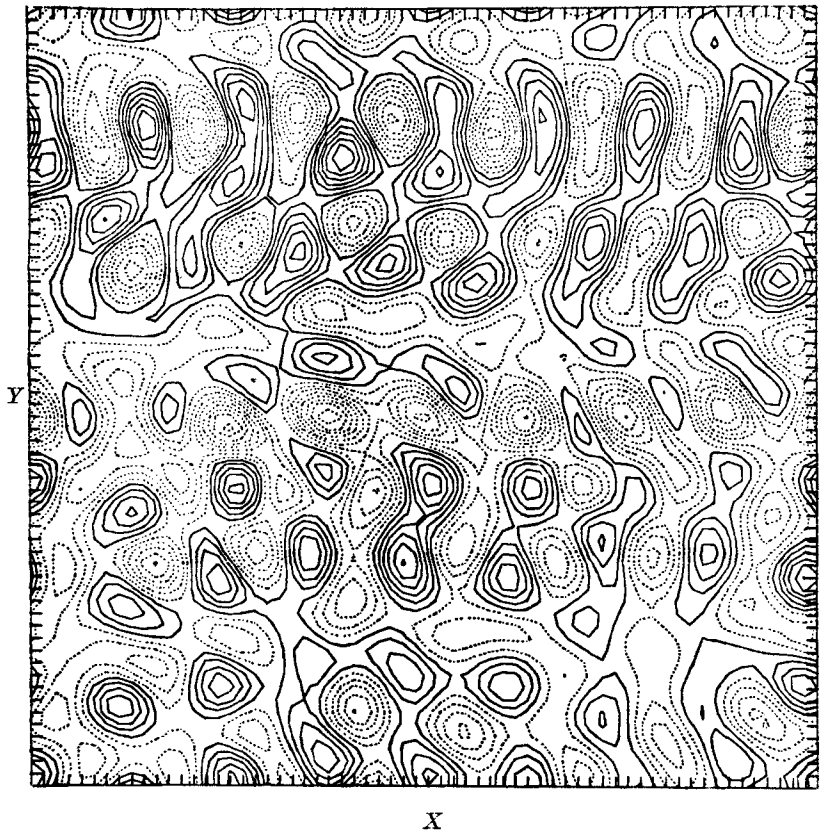

FIGURE 5. Stream function ψ after 50 time steps of forcing. The decay experiment for the high Reynolds number case, $R = 537$, starts at this point.

wavelength and amplitude of the forcing function are both arbitrarily set equal to unity and the viscosity coefficient $\nu = 2{\cdot}5 \times 10^{-4}$. All quantities should be considered dimensionless and the only fundamental adjustable parameter is a Reynolds number, as defined below.

The remaining curves in figure 6 each consist of energy spectra obtained by averaging between the 1000th and 1200th steps of time integration of (22), including 10–50 steps of initial forcing. The spectra are labelled according to the Reynolds number at the 1100th time step, as defined by

$$R = \bar{E}^{\frac{1}{2}} L/\nu, \tag{23}$$

where

$$L = \bar{E}^{\frac{1}{2}}/\eta^{\frac{1}{3}}.$$

The quantity η is the viscous dissipation of enstrophy. Our identification of R as the Reynolds number depends on the fact that L is an appropriate macroscale in two-dimensional turbulence, analogous to $\bar{E}^{\frac{3}{2}}/\epsilon$ in three dimensions, where ϵ

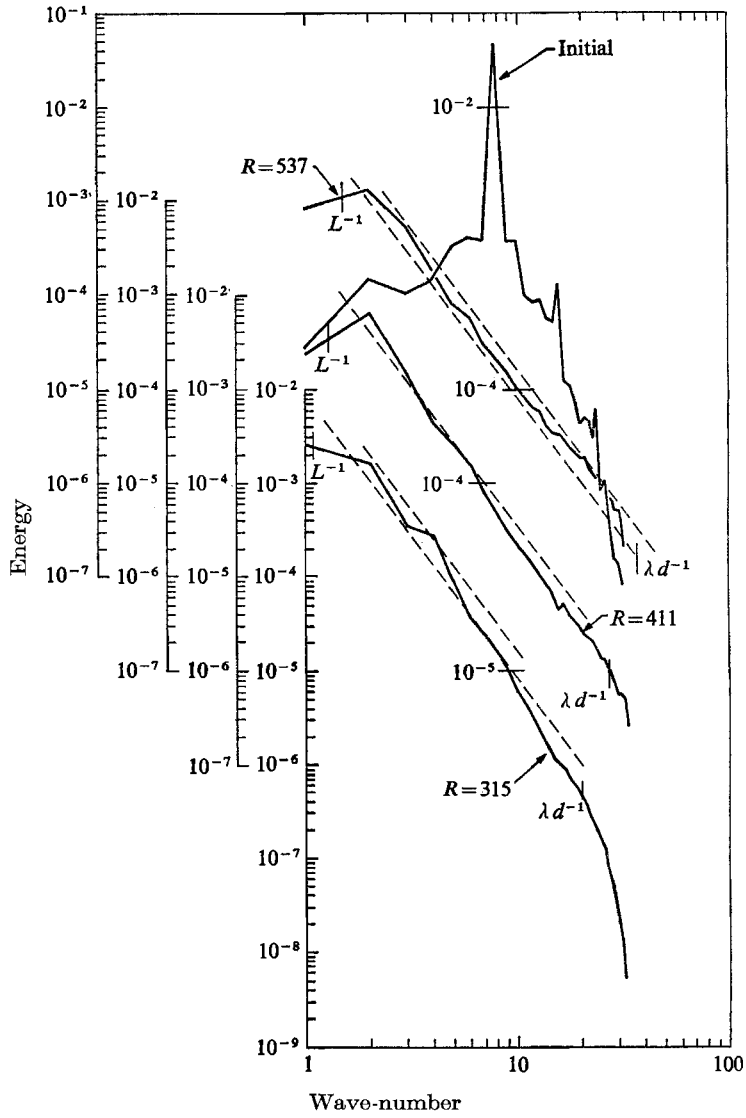

FIGURE 6. Scalar energy spectrum corresponding to the stream field of figure 1, labelled 'initial'. Energy spectra for three realizations, each averaged between the 1000th and 1200th time steps and labelled according to the Reynolds number defined by equation (23).

is the energy dissipation. The spectrum function for the highest Reynolds number exhibits an extensive region of -3 slope that is consistent with Kraichnan's, Leith's and Batchelor's predictions. The depression of the tail for the lower R cases is probably due to the viscous cut-off, while its slight enhancement for the high R case can be attributed to finite difference errors. The vertical lines are

the values of L^{-1} and λ_d^{-1}, where λ_d is the nominal dissipation scale for two-dimensional turbulence, given by

$$\lambda_d = (\nu^3/\eta)^{\frac{1}{6}}. \tag{24}$$

Let us now assume that the scalar energy spectrum is adequately approximated by the power-law expression suggested by Batchelor, i.e.

$$E(k) = \beta\eta^{\frac{2}{3}}k^{-3}, \quad k_c < k < k_d, \tag{25}$$

where k_c and k_d are lower and upper wave-number limits, which may be functions of time, and β is a possibly universal constant. The total energy, enstrophy and enstrophy dissipation rate can then be described in terms of integrals of the scalar energy spectrum as

$$\bar{E} = \int_0^\infty E(k)\,dk, \quad \bar{S} = \int_0^\infty k^2 E(k)\,dk, \quad \eta = \nu\overline{\left(\frac{\partial\zeta}{\partial x_i}\right)^2} = 2\nu\int_0^\infty k^4 E(k)\,dk. \tag{26}$$

Upon substitution of the spectrum of (25) into the first and third of these and integration over its nominal range, we find that k_c and k_d are related to L and λ_d by

$$k_c L = (\tfrac{1}{2}\beta)^{\frac{1}{2}}, \quad k_d\lambda_d = \beta^{-\frac{1}{2}}. \tag{27}$$

From figure 6 it is evident that L and λ_d are closely associated with the limits of the inertial range.

The results of these experiments allow for an empirical determination of β, the dimensionless constant of (25). If we assume that each of the spectral amplitudes shown in figure 6 represents the kinetic energy contained in the scalar wave-number band of width Δk centred around scalar wave-number k, (25) can be solved for β as follows:

$$\beta = \frac{k^3/\Delta k}{\eta^{\frac{2}{3}}}\int_{k-\frac{1}{2}\Delta k}^{k+\frac{1}{2}\Delta k} E(k)\,dk. \tag{28}$$

For comparison with the analytic theories based on definition of spectra as circle integrals in phase space, (28) is evaluated with k replaced by k_{eff}, the r.m.s. wave-number of the components going into the box averages. Under the assumption that energy is equally divided among all the possible components of the box average it is easily verified that $k_{\text{eff}} = 1{\cdot}13k$, and this conversion factor is uniformly applied. Figure 7 shows time plots of β for the three computation experiments described above, based on evaluation of (28) at wave-number 6. Similar plots were also made at wave-numbers 10 and 16, with essentially similar results. The average value of β for the latter part of the time records is near 2·0. The calculations for forced turbulence, described in I, indicated values of β near 4·0. The discrepancy is unexplained, although the present values might be considered more reliable because of the greater range of the k^{-3} spectrum associated with them. In the next section we describe another possible explanation.

Batchelor predicts the time-dependent behaviour of the principle quadratic parameters in decaying two-dimensional turbulence as

$$\bar{S} = \tfrac{1}{2}At^{-2}, \tag{29}$$

and

$$\eta = At^{-3}, \tag{30}$$

where A is a constant. Since the energy dissipation is proportional to enstrophy we may also write

$$\bar{E} = \bar{E}_\infty - \nu A t^{-1}, \tag{31}$$

where $\bar{E}_\infty$ is the energy which is trapped at the largest scales after development of an extensive k^{-3} spectrum. Figure 8 shows curves of these parameters against

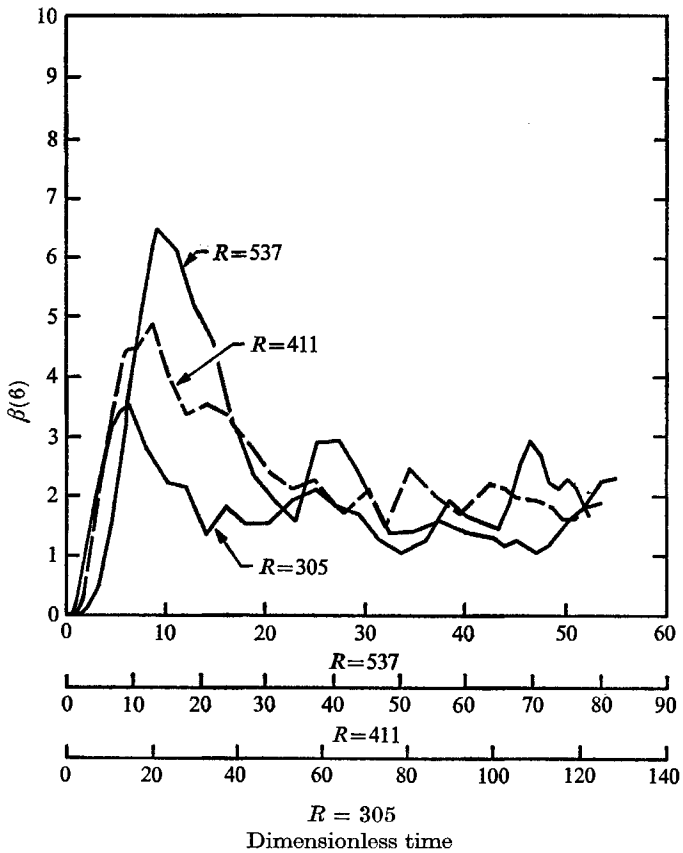

FIGURE 7. The dimensionless spectrum function constant, β, calculated from the wave-number 6 energy amplitude for three Reynolds number experiments.

time for the high Reynolds number case, together with expressions of the form of (29)–(31), but with an arbitrary time origin. The values of A and the time origin, say t_0, are those which best satisfy $2(t-t_0)^2\bar{S} = (t-t_0)^3\eta = A =$ constant for the last few hundred time steps. It is then found that $\bar{E}_\infty = \bar{E} + A\nu t^{-1}$ also becomes essentially constant during that period. As shown on figure 8, $t_0 = -4{\cdot}0$ and $\bar{E}_\infty = 0{\cdot}0221$ for this case. The constant A is found to be ~ 1250. From the figure it appears that the predictions of (29)–(31) are well verified by our results, but in the next section we point out an apparent inconsistency of these predictions.

4. The question of the 'logarithmic correction terms'

Kraichnan pointed out that the enstrophy cascade in two-dimensional turbulence differs in an important respect from the analogous energy cascade in three

dimensions. In two dimensions, as Reynolds number approaches infinity, the total enstrophy diverges logarithmically, with each octave adding an equal contribution. Kraichnan argued that in this circumstance the cascade interactions cannot be considered local in wave vector space and proposed that the k^{-3} spectrum should be modified by logarithmic correction terms. He also anticipated that β would not likely be as universal a constant as that of the Kolmogoroff

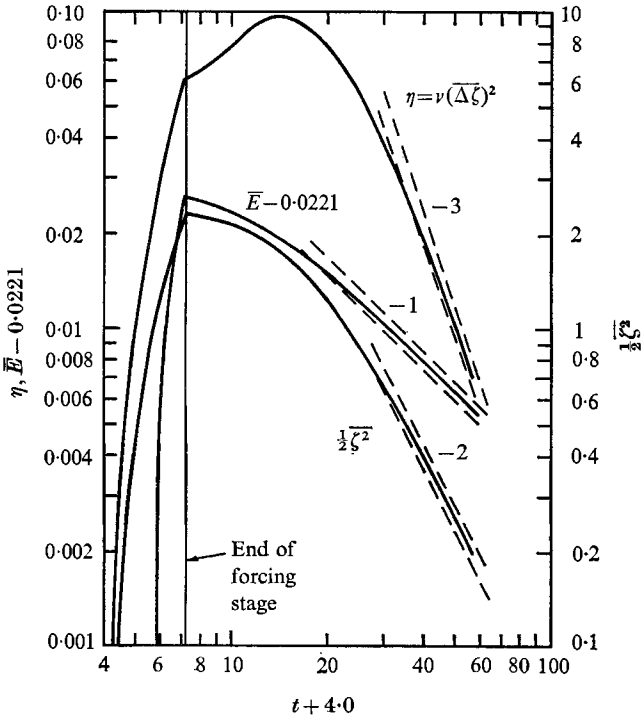

FIGURE 8. Average energy, $\bar{E}$, average enstrophy $\frac{1}{2}\overline{\zeta^2}$ and average enstrophy dissipation, η, as functions of time for the high Reynolds number case. Batchelor's theoretical predictions are shown as the dashed power law lines.

spectrum, but might depend on the nature of driving forces. Batchelor did not discuss this point, except to mention the logarithmic divergence of the total enstrophy with increasing R. It is clear, however, that this divergence leads to an inconsistency in Batchelor's analysis. If we eliminate time from (29) and (30) and evaluate the remaining terms by substitution of (25) into (26) we find that

$$A^{\frac{1}{2}} = 2\bar{S}/\eta^{\frac{1}{2}} = 2\beta \ln (k_d/k_c). \tag{32}$$

From (23), (24), (27) and (30), however, the ratio k_d/k_c increases like $t^{\frac{1}{12}}$ in the decay process, so evidently A cannot be constant.

Although Kraichnan did not suggest a form for the logarithmic correction, in order to make Batchelor's dimensional analysis valid it appears to be necessary to find one such that enstrophy approaches a constant as $R \to \infty$. One of the simplest such forms is

$$E(k) = \frac{\beta \eta^{\frac{2}{3}} k^{-3}}{1+\gamma^2(\ln k/k_c)^2}, \tag{33}$$

where γ is another dimensionless constant. By substitution of this relation into (26) we find that total enstrophy is given by

$$\bar{S} = \frac{\beta \eta^{\frac{2}{3}}}{\gamma} \tan^{-1}[\ln(k_d/k_c)]. \tag{34}$$

The other principal moments, total energy and enstrophy dissipation, are more difficult to evaluate in this case but remain convergent as $k_d/k_c \to \infty$. The slope of the energy spectrum on log–log paper becomes everywhere steeper than -3, with maximum steepness given by

$$-\frac{d[\ln E(k)]}{d[\ln k]}\bigg|_{\max} = 3+\gamma \quad \text{at} \quad \frac{k}{k_c} = e^{1/\gamma}. \tag{35}$$

Since we now have bounded enstrophy, Batchelor's constant becomes independent of R in the infinite limit, i.e.

$$A^{\frac{1}{3}} = \beta\pi/\gamma \quad \text{at} \quad k_d/k_c = \infty. \tag{36}$$

Using a different argument Kraichnan (1970) has postulated a logarithmic correction term of the form

$$E(k) = \beta \eta^{\frac{2}{3}} k^{-3} [\ln(k/k_c)]^{-\frac{1}{3}}.$$

The available resolution of the numerical solution described here is inadequate to test the validity of either of Kraichnan's predictions or equation (33). There is some indication, however, of a slope somewhat steeper than -3 in the intermediate Reynolds number spectrum in figure 6 at wave-numbers much lower than λ_d [1].

5. Correlation functions

The most important of the Eulerian correlation functions for two-dimensional isotropic turbulence appear to be the two-point longitudinal and transverse velocity correlations and the two-point isotropic vorticity correlation, defined respectively as

$$f(r) = [\overline{u_1(\mathbf{x}+\mathbf{i}_1 r)\, u_1(\mathbf{x})} + \overline{u_2(\mathbf{x}+\mathbf{i}_2 r)\, u_2(\mathbf{x})}]/\overline{u_i^2}, \tag{37}$$

$$g(r) = [\overline{u_1(\mathbf{x}+\mathbf{i}_2 r)\, u_1(\mathbf{x})} + \overline{u_2(\mathbf{x}+\mathbf{i}_1 r)\, u_2(\mathbf{x})}]/\overline{u_i^2}, \tag{38}$$

$$z(r) = \overline{\zeta(\mathbf{x}+\mathbf{r})\, \zeta(\mathbf{x})}/\overline{\zeta^2}. \tag{39}$$

Figures 9–11 show f, g and z for separations of up to one-half the computational area dimension, averaged over all space and over the 200 time steps of each experiment for which the spectral plots are exhibited. Because of the periodicity of the computational area the correlations for larger separation distances are simply mirror images of those shown. In isotropic turbulence the above functions are expected to be related by

$$g = (rf')', \tag{40}$$

$$z = r^{-1}[r(f+g)']'/8f''(0). \tag{41}$$

Rough comparisons (not shown here) indicate that the above relations are reasonably well satisfied by our computed correlation functions except at the larger separations, where the functions are obviously not well determined by the present computations. The longitudinal integral scale, $\int f(r)\,dr$, averages to about 1·2. This may be compared to the macro-scale L used for calculating the Reynolds number, which has an average value for the last 200 steps of the three experiments near 0·95.

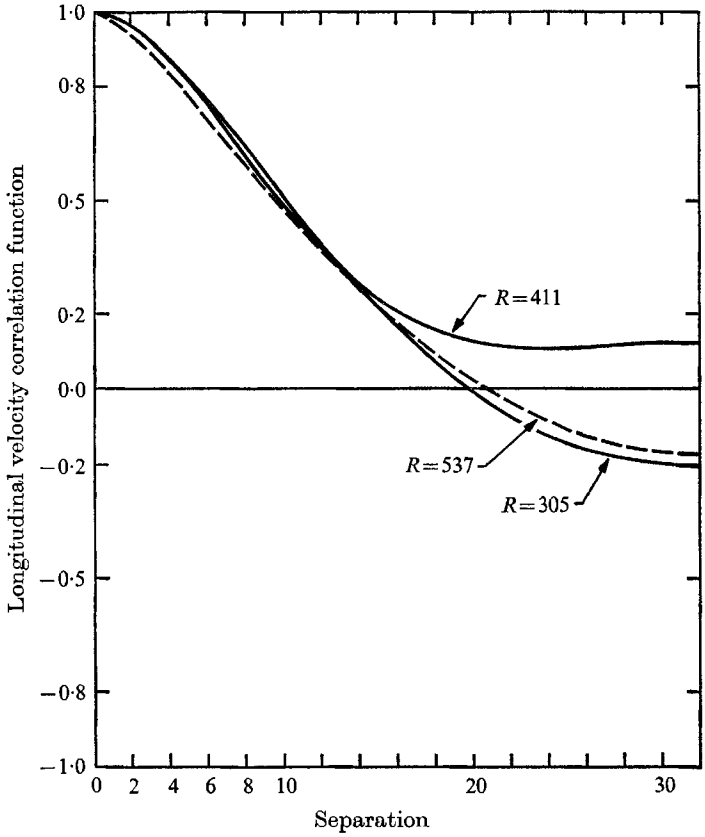

FIGURE 9. The longitudinal velocity correlation, $f(r)$, for all three experiments as a function of separation distance r, averaged between the 1000th and 1200th time steps.

6. Deviations from Gaussianity

Figures 12 and 13 show the stream function and vorticity at the 1000th time step for the lowest Reynolds number case. The stream function is dominated by the large scale components. The vorticity field, however, shows much small scale structure, which is consistent with the fact that equal amounts of enstrophy are contributed by each octave of a k^{-3} energy spectrum function. From figure 13 one gains an impression of considerable intermittency in the field of vorticity and its gradient. An objective measure of the intermittency of a field is given by its deviation from Gaussianity. We have therefore computed the variance, skewness

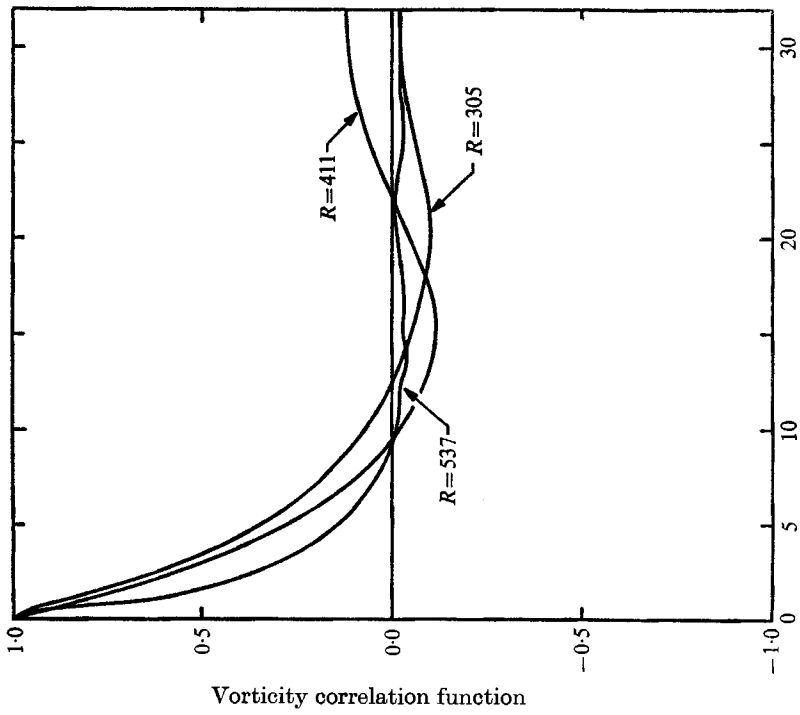

FIGURE 11. The isotropic vorticity correlation function $z(r)$.

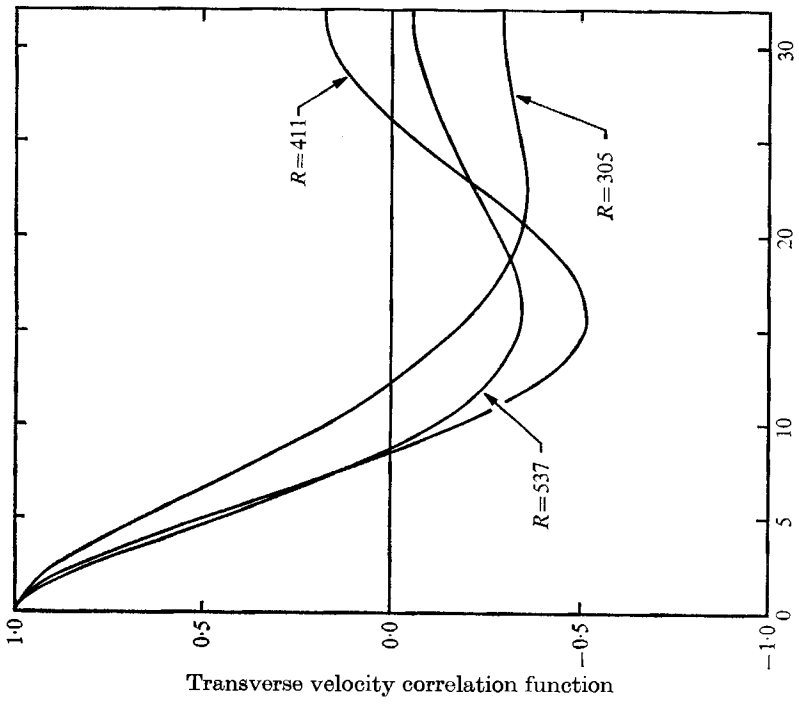

FIGURE 10. The transverse velocity correlation function $g(r)$.

and flatness factor of the velocity, vorticity and vorticity gradient fields for the three simulation experiments as a function of time.

Figure 14 shows the time record of the flatness factor of u_1, u_2, ζ, $\partial\zeta/\partial x_1$, and $\partial\zeta/\partial x_2$ for the low Reynolds number case. The flatness factor of a field $f(x,t)$ is

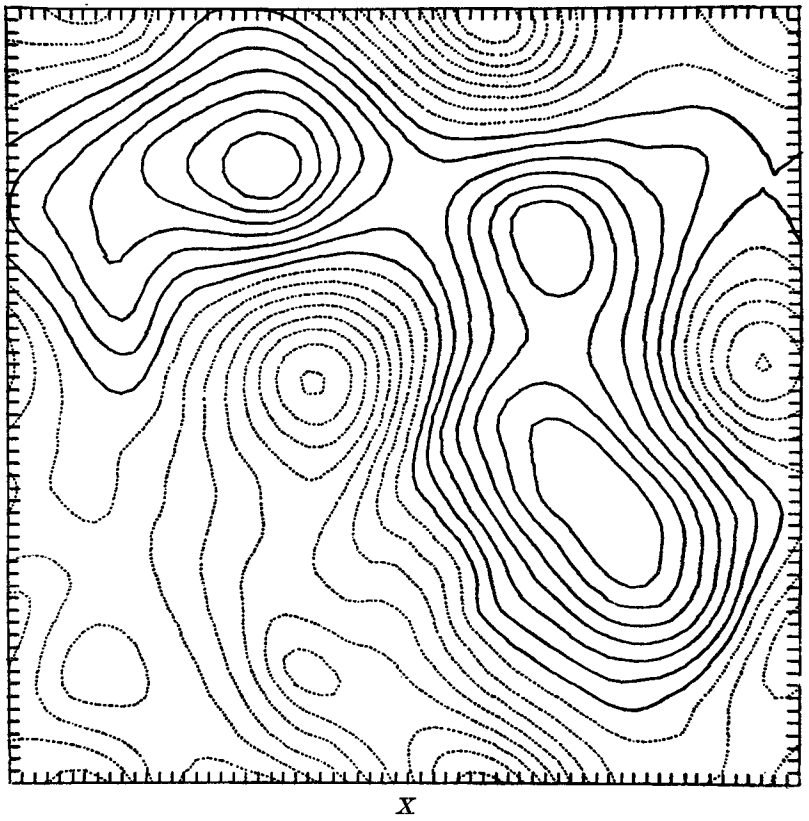

FIGURE 12. Stream function at the 1000th time step for the low Reynolds number experiment.

here defined as $\overline{f^4}/\overline{f^2}^2$ and is known to equal 3 for a Gaussian field. From figure 14 we see that the initial velocity fields appear Gaussian, but as the decay spectrum develops they exhibit a slight sub-Gaussian flatness. On the other hand the flatness factors for the vorticity and vorticity gradient fields become greater than 3. The reduced value for the velocity field flatness can probably be explained by the tendency of the stream function to approach a single sinusoidal mode, for which the velocity field flatness can be shown to lie between 1·5 and 2·25, depending on its isotropy. The flatness factor for the vorticity gradients is quite large and indicates a strong tendency for intermittency to develop in the enstrophy dissipation field. The flatness factors of u_1 and u_2 and for the x_1 and x_2 derivatives of vorticity are presumably random, although they tend to be rather persistent. Similarly the skewness values which have been computed (but not shown here) for the various fields all appear to oscillate around zero, but with considerable persistence in their deviations.

The results for the higher Reynolds number experiments differ significantly from those illustrated in figure 14 in that the flatness factor of the vorticity gradient field is substantially less, and in fact is smaller than that of the vorticity.

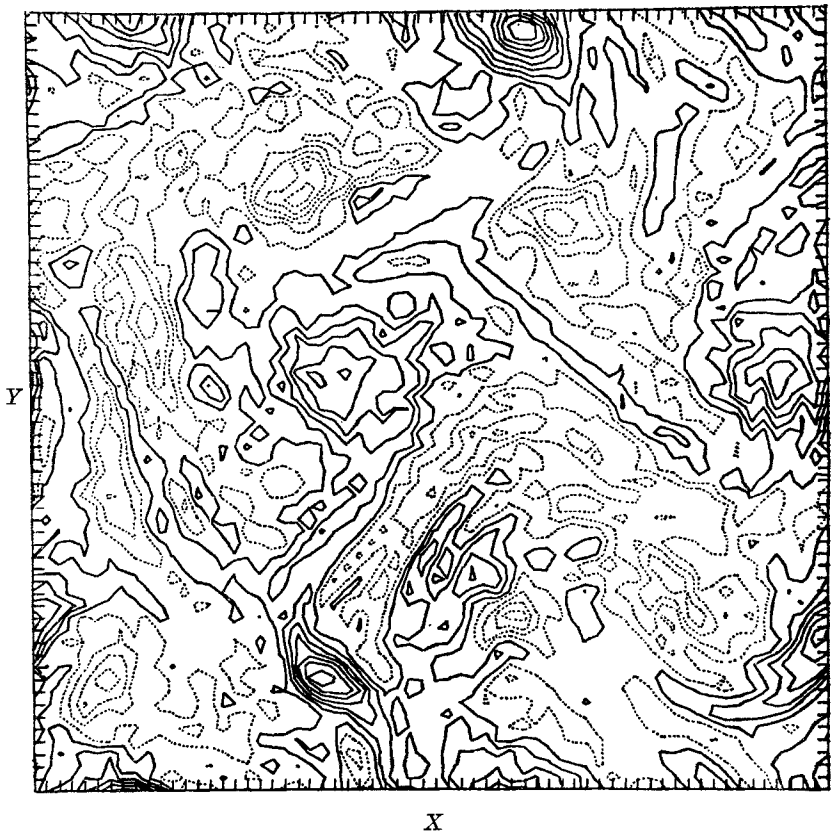

FIGURE 13. Vorticity at the 1000th time step for the low Reynolds number experiment.

This result is apparently spurious, due to the truncation error introduced by computing these gradients from finite difference approximations. We conclude that the numerical resolution used here is insufficient to allow for definitive measurements of these statistical properties when the Reynolds number is large enough for a well defined k^{-3} spectrum region to exist.

7. Conclusions

The work described in this paper tends to confirm, for the most part, the recent theoretical studies of two-dimensional turbulence, at least to the extent that they agree with each other. In two-dimensional flow, a 'cascade' of enstrophy occurs through the smaller scales of motion and forms an enstrophy inertial range, characterized by a scalar energy spectrum proportional to k^{-3} or steeper. In several respects the enstrophy cascade and inertial range are analogous to those of energy in three dimensions, but there are notable differences. In the early

stages of development of turbulent flow from Gaussian initial conditions, a vorticity gradient is generated by self-distortion of the flow. We may compare this process with the vortex stretching which produces vorticity and turbulence in

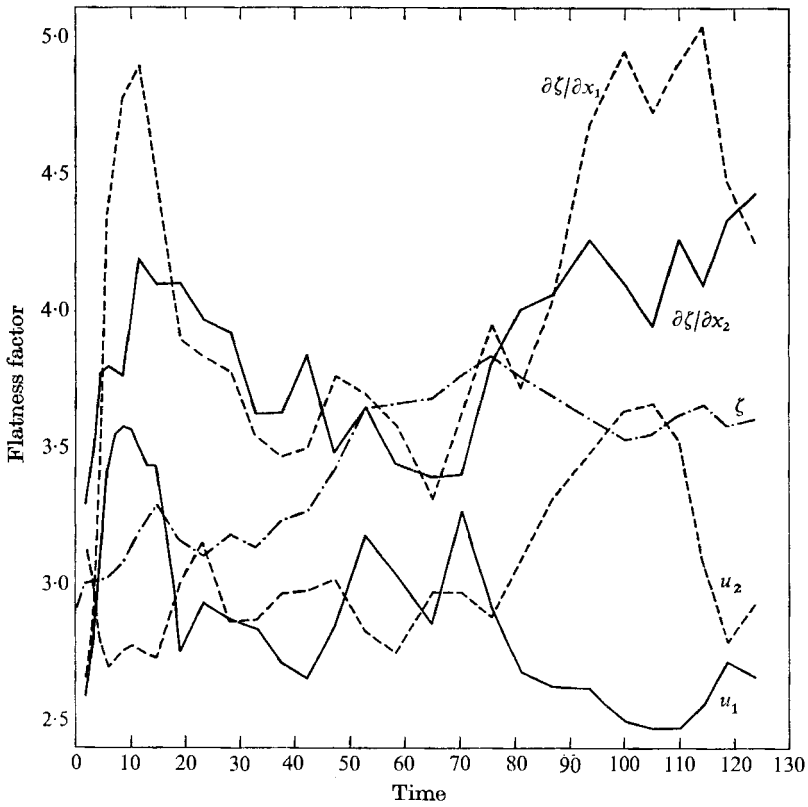

FIGURE 14. Flatness factors of the fields of u_1, u_2, ζ, $\partial\zeta/\partial x_1$ and $\partial\zeta/\partial x_2$ as functions of time for the low Reynolds number experiment.

three dimensions. In both cases the quasi-normality assumption leads to a prediction that is probably valid for a limited period of time. The prediction for the three-dimensional case is (Proudman & Reid 1954) simply that

$$d^2(\overline{\omega^2})/dt^2 = \tfrac{1}{3}(\overline{\omega^2})^2, \tag{42}$$

where ω is the vorticity amplitude. Equation (18), the comparable result for two-dimensional flow, is somewhat more complex, however, presumably due to the additional constraints on non-linear interactions in two dimensions.

The power-law prediction for the energy spectrum and the presumed universal constant are somewhat shakier concepts in two-dimensional than three-dimensional turbulence, due to the logarithmic divergence of enstrophy as $R \to \infty$ and to the related non-localness of the spectral interactions. The logarithmic correction proposed in (33) appears to be a partial solution to the internal inconsistency of the k^{-3} spectrum but remains purely speculative at this time.

The deviations from Gaussianity found in the vorticity gradient statistics are apparently completely analogous to the non-Gaussianity found in the velocity

gradient statistics in three-dimensional turbulence (Stewart, Wilson & Burling 1970; Gibson, Stegen & Williams 1970). Enstrophy dissipation, like energy dissipation in three dimensions, apparently tends toward intermittency, with possibly a log-normal distribution function at high Reynolds numbers.

One of the most important conclusions of the present work is that numerical simulation is now apparently capable of adding to our fundamental understanding of turbulent processes at a reasonable cost. The computations reported here consumed only about 10 h of computing time on a CDC 6600, including a number of preliminary, irrelevant and additional experiments not mentioned above. Problems of a purely numerical nature, such as computational stability, aliasing and truncation errors, did occur in some of the earlier experiments but were not of sufficient magnitude to seriously interfere with the final results. Significant improvements could be obtained at moderate additional cost by integrating the spectral equations with the aid of fast Fourier transforms, as outlined by Orszag (1969). Such techniques are probably necessary if simulation methods are to be applied to the much more formidable problem of three-dimensional turbulence.

This work could not have been completed without the computer programming assistance ably provided by David W. Fulker. Useful comments and encouragement were received from C. E. Leith, J. W. Deardorff, D. G. Fox and Steven A. Orszag. The reviewers, including R. Kraichnan and G. K. Batchelor, added extremely useful comments, leading to substantial revisions and improvements of the paper.

The National Center for Atmospheric Research is sponsored by the National Science Foundation.

REFERENCES

ARAKAWA, A. 1966 Computational design for long-term numerical integration of the equations of fluid motion. Two-dimensional incompressible flow. Part 1. *J. Comp. Phys.* **1**, 119–143.

BATCHELOR, G. K. 1969 Computation of the energy spectrum in homogeneous two-dimensional turbulence. High-speed computing in fluid dynamics. *Phys. Fluids Suppl.* II, 233–239.

GIBSON, C. H., STEGEN, G. R. & WILLIAMS, R. B. 1970 Statistics of the time structure of turbulent velocity and temperature fields measured at high Reynolds number. *J. Fluid Mech.* **41**, 153–167.

KRAICHNAN, R. 1962 The closure problem of turbulence theory. *Proc. Symposium Appl. Math.* **13**, 199–225.

KRAICHNAN, R. 1967 Inertial ranges in two-dimensional turbulence. *Phys. Fluids*, **10**, 1417–1423.

KRAICHNAN, R. 1970 Inertial-range transfer in two- and three-dimensional turbulence. To be published.

LEITH, C. E. 1968 Diffusion approximation for two-dimensional turbulence. *Phys. Fluids*, **11**, 671–674.

LILLY, D. K. 1969 Numerical simulation of two-dimensional turbulence. High-speed computing in fluid dynamics. *Phys. Fluids Suppl.* II, 240–249.

OGURA, Y. 1952 The structure of two-dimensionally isotropic turbulence. *J. Meteor. Soc. Japan*, **30**, 59–64.

OGURA, Y. 1958 On the isotropy of large scale disturbances in the upper troposphere. *J. Meteor.* **15**, 375–382.

OGURA, Y. 1962 Energy transfer in a normally distributed and isotropic turbulent velocity field in two dimensions. *Phys. Fluids*, **5**, 395–401.

ORSZAG, S. A. 1969 Numerical methods for the simulation of turbulence. *Phys. Fluids Suppl.* II, 250–257.

PROUDMAN, I. & REID, W. H. 1954 On the decay of a normally distributed and homogeneous turbulent velocity field. *Phil. Trans. Roy. Soc.* A **247**, 163–189.

REID, W. H. 1955 On the stretching of material lines and surfaces in isotropic turbulence with zero fourth cumulants. *Proc. Cam. Phil. Soc.* **51**, 350–361.

STEWART, R. W., WILSON, J. R. & BURLING, R. W. 1970 Some statistical properties of small-scale turbulence in an atmospheric boundary layer. *J. Fluid Mech.* **41**, 141–152.